Dual emission from Mn(II) complexes with carbazolyl-substituted phosphoramides

M. Bortoluzzi [a,b,*], J. Castro [c], V. Ferraro [a]

[a] Dipartimento di Scienze Molecolari e Nanosistemi, Università Ca' Foscari Venezia, 30172 Mestre, VE, Italy
[b] Consorzio Interuniversitario Reattività Chimica e Catalisi (CIRCC), via Celso Ulpiani 27, 70126 Bari, Italy
[c] Departamento de Química Inorgánica, Universidade de Vigo, Facultade de Química, Edificio de Ciencias Experimentais, 36310 Vigo, Galicia, Spain

ARTICLE INFO

Keywords:
Manganese
Tetrahedral complexes
Photoluminescence
Phosphoramide
Carbazole

ABSTRACT

The carbazolyl-substituted phosphoramide *N*,*N*,*N*′,*N*′-tetramethyl-*P*-carbazol-9-ylphosphonic diamide (L) was successfully coordinated to MnX_2 halides (X = Cl, Br, I), obtaining tetrahedral complexes having general formula $[MnX_2L_2]$. The structures were ascertained by means of single-crystal X-ray diffraction. The three complexes show appreciable luminescence in the visible range upon excitation with UV radiation, attributed to the Mn(II) $^4T_1(^4G)\rightarrow{}^6A_1(^6S)$ transition superimposed to the emission from coordinated ligands. The different contributions are particular evident for the chloro-complex and the relative intensity depends upon the excitation wavelength. The correlation between the two emitting levels is highlighted by the luminescence decay curves of the three compounds.

1. Introduction

The metal-centred luminescence of $[MnX_4]^{2-}$, $[Mn_3X_{12}]^{6-}$ and $[MnX_3]_n^{n-}$ anionic halide species is of actual interest for advanced technology applications, such as sensors, OLEDs, optical waveguides, nonlinear optics, X-ray scintillators and multifunctional devices [1–20]. The luminescence performances of these compounds, commonly defined as organic–inorganic hybrids, strongly depend upon the choice of the organic counter-cation.

Noticeable luminescence is observable also by replacing the halides with suitable species in the Mn(II) coordination sphere, and the most applied ligands in this field are O-donors based on pentavalent phosphorus [21,22]. The use of triphenylphosphine oxide allowed the isolation of the tetrahedral complex $[MnBr_2(O{=}PPh_3)_2]$ [23], of current interest because of its ferroelectric properties and triboluminescence [24–26]. The introduction of substituents such as -NMe_2, -OMe and -CF_3 on one of the phenyl rings of triphenylphosphine oxide causes the variation of emission maximum and luminescence lifetime, and the related Mn(II) halide complexes are applicable for luminescent printing [27].

Besides the possible energy transfer from the phosphorous-bonded organic fragments to Mn(II), the substituents on the phosphorus atom can influence the final geometry of the complexes and therefore their luminescence features. In particular, the coordination of polydentate phosphine oxides to Mn(II) afforded in recent years mono-, di- and polynuclear complexes with coordination numbers from four to six. The emissions fall from the green to the red regions of the visible spectrum, depending upon the coordination geometry [28–30]. Among the most intriguing features, luminescent vapochromism and thermochromism, triboluminescence, polymorphic luminescence, dual emission and excitation-dependent luminescence must be cited [31–37]. The tetrahedral complex $[MnBr_2(BDFDPO)]$ (BDFDPO = 4,6-bis(diphenylphosphino)dibenzofuran dioxide) was successfully applied as active material in OLEDs [38], while the ligand (9,9-dimethyl-9*H*-xanthene-4,5-diyl)bis(diphenylphosphine oxide) (DDXPO) allowed the isolation of the luminescent five-coordinated complex $[MnBr(DDXPO)_2]Br$, suitable as scintillator for X-ray detection [39].

Our research group is currently studying [O=P]-donor ligands alternative to phosphine oxides as suitable ligands for the sensitization of Mn(II) luminescence. Green-emitting mono- and polynuclear tetrahedral complexes with aromatic phosphoramidates and phosphonates were recently synthesized, some of them characterized by high photoluminescence quantum yields, despite the scarce absorption features [40]. Another group of tetrahedral Mn(II) luminescent complexes was isolated by using phosphoramides, arylphosphonic diamides and related species [41–45]. As already observed for the phosphine oxides, aromatic

* Corresponding author.
E-mail address: markos@unive.it (M. Bortoluzzi).

Accepted 4 March 2022

fragments directly bonded to the phosphorus atom can enhance Mn(II) luminescence because of the light-harvesting behaviour and the possibility of ligand-to-metal energy transfer. Such a possibility is however deeply related to the electronic structure of the aromatic group chosen. The formal replacement of the P-bonded phenyl of $O{=}PPh(NMe_2)_2$ with indol-1-yl caused an overall enhancement of emission from the related complexes because of the increased light-harvest, while excitation-dependent dual emission was observed by introducing the 2-naphthyl substituent in the skeleton of the ligand.

In order to further investigate the role of aromatic substituents in the sensitization of Mn(II) luminescence, the research on phosphoramides functionalized with light-harvesting substituents was recently focused on species containing the carbazolyl fragment. It is worth noting that carbazolylphosphines and carbazolylphosphine oxides were recently considered as suitable materials for OLEDs fabrication [46–48]. In this paper we report the synthesis, characterization and photoluminescence of tetrahedral complexes obtained by reacting Mn(II) halides with *N*,*N*,*N*′,*N*′-tetramethyl-*P*-carbazol-9-ylphosphonic diamide. The ligand (L) is depicted in Chart 1 for clarity.

2. Experimental part

2.1. Materials and methods

Commercial solvents (Merck) were purified as described in the literature [49]. Anhydrous MnX_2 halides (X = Cl, Br, I) were purchased from Alfa Aesar. The organic reactants were Merck products, used as received. *N*,*N*,*N*′,*N*′-tetramethyl-*P*-carbazol-9-ylphosphonic diamide (L) was synthesized on the basis of a reported procedure [50]. The syntheses of the Mn(II) complexes were carried out under an inert atmosphere, working in a glovebox (MBraun Labstar with an MB 10 G gas purifier) filled with N_2.

Elemental analyses (C, H and N) were carried out using an Elementar Unicube microanalyzer. Halide contents were determined using Mohr's method [51]. Magnetic susceptibilities were measured on solid samples at 298 K using an MK1 magnetic susceptibility balance (Sherwood Scientific Ltd) and corrected for diamagnetic contribution by means of tabulated Pascal's constants [52]. Melting points were determined using a modified FALC 360 D instrument equipped with a camera. Conductivity measurements were carried out using a Radiometer Copenhagen CDM83 instrument. IR spectra were collected in the range of 4000–400 cm^{-1} using a PerkinElmer Spectrum One spectrophotometer. NMR spectra were collected using a Bruker Avance 300 instrument operating at 300.13 MHz of the ^1H resonance. ^1H NMR spectra were referred to the partially non-deuterated fraction of the solvent, itself quoted to tetramethylsilane. $^{31}P\{^1H\}$ NMR resonances were referred to 85% H_3PO_4 in water.

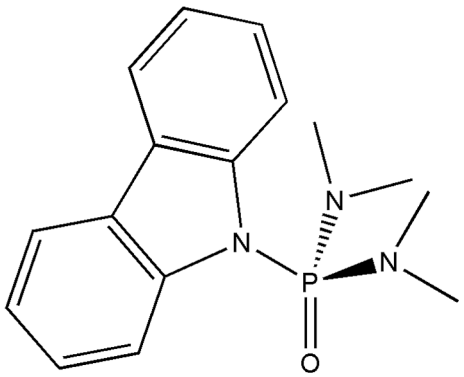

Chart 1. *N*,*N*,*N*′,*N*′-tetramethyl-*P*-carbazol-9-ylphosphonic diamide (L).

2.2. Synthesis of the complexes

The $[MX_2L_2]$ complexes (X = Cl, Br, I) were isolated by slowly adding a solution containing 2.1 mmol (0.633 g) of L dissolved in 10 ml of EtOH into another solution of the proper anhydrous manganese salt MnX_2 (1.0 mmol: 0.126 g for $MnCl_2$, 0.215 g for $MnBr_2$ and 0.309 g for MnI_2) dissolved in 20 ml of EtOH. The reaction mixture was stirred overnight inside the glove-box at room temperature. The solvent was then evaporated under reduced pressure and the solid thus obtained was dissolved in the minimum amount of dichloromethane. The solution was cleared by centrifugation and the solvent was removed under reduced pressure. The product isolated by addition of diethyl ether was then filtered and dried *in vacuo*. Yields: 0.583 g (80%) for **$[MnCl_2L_2]$**, 0.695 g (85%) for **$[MnBr_2L_2]$**, 0.620 g (68%) for **$[MnI_2L_2]$**. Crystals suitable for X-ray diffraction were obtained from dichloromethane/diethyl ether solutions.

$[MnCl_2L_2]$. Anal. calcd for $C_{32}H_{40}Cl_2MnN_6O_2P_2$ (728.49 g mol^{-1}, %): C, 52.76; H, 5.53; N, 11.54; Cl, 9.73. Found (%): C, 52.55; H, 5.55; N, 11.49; Cl, 9.77. M.p. 205 °C. χ_M^{corr} (c.g.s.u.): $1.48{\cdot}10^{-2}$. Λ_M (CH_2Cl_2, 298 K): <2 ohm^{-1} mol^{-1} cm^2. IR (KBr, cm^{-1}): 3120–3000 m/w (aromatic $\nu_{C\text{-}H}$), 2930–2800 m ($\nu_{C\text{-}H}$), 1650–1600 m (aromatic $\nu_{C\text{-}C}$ and $\nu_{C\text{-}N}$), 1200–1120 s ($\nu_{P\text{-}O}$ and $\nu_{C\text{-}N}$), 1030–970 s ($\nu_{P\text{-}N}$). ^1H NMR ($CDCl_3$, 298 K) δ 8.41 broad, 7.25 broad (carbazole). $^{31}P\{^1H\}$ NMR ($CDCl_3$, 298 K) δ 16.31 s (broad).

$[MnBr_2L_2]$. Anal. calcd for $C_{32}H_{40}Br_2MnN_6O_2P_2$ (817.39 g mol^{-1}, %): C, 47.02; H, 4.93; N, 10.28; Br, 19.55. Found (%): C, 46.83; H, 4.95; N, 10.32; Br, 19.47. M.p. 210 °C. χ_M^{corr} (c.g.s.u.): $1.57{\cdot}10^{-2}$. Λ_M (CH_2Cl_2, 298 K): <2 ohm^{-1} mol^{-1} cm^2. IR (KBr, cm^{-1}): 3080–3000 m/w (aromatic $\nu_{C\text{-}H}$), 2980–2820 m ($\nu_{C\text{-}H}$), 1640–1390 m (aromatic $\nu_{C\text{-}C}$ and $\nu_{C\text{-}N}$), 1200–1120 s ($\nu_{P\text{-}O}$ and $\nu_{C\text{-}N}$), 1030–970 s ($\nu_{P\text{-}N}$). ^1H NMR ($CDCl_3$, 298 K) δ 8.64 broad, 7.23 broad (carbazole). $^{31}P\{^1H\}$ NMR ($CDCl_3$, 298 K) not detected.

$[MnI_2L_2]$. Anal. calcd for$C_{32}H_{40}I_2MnN_6O_2P_2$ (911.39 g mol^{-1}, %): C, 42.17; H, 4.42; N, 9.22; I, 27.85. Found (%): C, 42.01; H, 4.44; N, 9.18; I, 27.74. M.p. 165 °C. χ_M^{corr} (c.g.s.u.): $1.51{\cdot}10^{-2}$. Λ_M (CH_2Cl_2, 298 K): <2 ohm^{-1} mol^{-1} cm^2. IR (KBr, cm^{-1}): 3060–3000 m/w (aromatic $\nu_{C\text{-}H}$), 2970–2820 m ($\nu_{C\text{-}H}$), 1640–1580 m (aromatic $\nu_{C\text{-}C}$ and $\nu_{C\text{-}N}$), 1203–1120 s ($\nu_{P\text{-}O}$ and $\nu_{C\text{-}N}$), 1030–930 s ($\nu_{P\text{-}N}$). ^1H NMR ($CDCl_3$, 298 K) δ 8.73 broad, 7.16 broad (carbazole). $^{31}P\{^1H\}$ NMR ($CDCl_3$, 298 K) not detected.

2.3. Crystal structure determination

The crystallographic data were collected at CACTI (Universidade de Vigo) at 100 K (CryoStream 800) using a Bruker D8 Venture Photon II CMOS detector and Mo-Kα radiation (λ = 0.71073 Å) generated by an Incoatec high brilliance IμS microsource. The software APEX3 [53] was used for collecting frames of data, indexing reflections, and the determination of lattice parameters, SAINT [53] for integration of the intensity of reflections, and SADABS [53] for scaling and empirical absorption correction. The crystallographic treatment was performed using the Oscail program [54], solved using the SHELXT program [55]. The structure was subsequently refined by a full-matrix least-squares methods based on F^2 using the SHELXL program [56]. Non-hydrogen atoms were refined with anisotropic displacement parameters. Hydrogen atoms were included in idealized positions and refined with isotropic displacement parameters. In the case of **$[MnI_2L_2]$** two molecules were found in the asymmetric unit, one of them showing some disorder on one of the methyl groups. A non-merohedral twinning was found in the last stages of the refinement, treated by using TWINROTMATR subroutine in PLATON [57]. The structures maintain high electronic densities in the final map. In the case of **$[MnCl_2L_2]$** attempts to eliminate the contributions to the diffraction pattern by using the squeeze routine [57] were unsuccessful, since the low quality of data [R_{int} = 0.1080 and a probably non-resolved twinning] does not allow to improve the model to satisfactory final indices. For this reason, the

geometrical parameters discussed below for this compound should be read with the appropriate caution. Other details concerning crystal data and structural refinement are given in Table 1. CCDC 2094660, 2094661 and 2094662 contain the supplementary crystallographic data for this paper. These data can be obtained free of charge from the Cambridge Crystallographic Data Centre via https://www.ccdc.cam.ac.uk/data_request/cif. PLATON (version 60720) [57] was used to obtain some geometrical parameters from the cif files.

2.4. Absorption and emission measurements

Absorption spectra of dichloromethane solutions were collected in the range of 235–700 nm using a PerkinElmer Lambda 40 spectrophotometer. Photoluminescence emission (PL) and excitation (PLE) measurements were carried out at room temperature on solid samples using a Horiba Jobin Yvon Fluorolog-3 spectrofluorometer. The compounds were stored in air-tight quartz sample holders, filled in a glovebox to avoid interaction of the complexes with moisture. A continuous-wave xenon arc lamp was used as the source, selecting the excitation wavelength using a double Czerny–Turner monochromator. A single grating monochromator coupled to a photomultiplier tube was used as the detection system for optical emission measurements. Excitation and emission spectra were corrected for the instrumental functions. Time-resolved analyses for Mn(II) complexes were performed in multi channel scaling (MCS) modality using pulsed UV LED sources (Horiba SpectraLED). In the case of the free *N,N,N′,N′*-tetramethyl-*P*-carbazol-9-ylphosphonic diamide lifetimes were recorded in TCSPC (time correlated single photon counting) mode employing an Horiba NanoLED centred at 373 nm. The observed lifetimes (τ_{obs}) of the excited states were determined from the mono-exponential fit of selected decay curves. The photoluminescence quantum yield (Φ) of the Mn(II) complexes in the solid state at room temperature was measured by means of an OceanOptics HR4000CG UV-NIR detector, fiber-coupled to an integrating sphere connected to an OceanOptics LED source centred at 365 nm. Values are reported as average of three measurements. Reflectance measurements were carried out with the sample OceanOptics spectrometer, coupled with an OceanOptics DH-2000-BAL tungsten/deuterium lamp. $BaSO_4$ was used as reflectance standard.

Table 1
Crystal data and structure refinement for $[MnX_2L_2]$.

Compound	**$[MnCl_2L_2]$**	**$[MnBr_2L_2]$**	**$[MnI_2L_2]$**
Empirical formula	$C_{32}H_{40}Cl_2MnN_6O_3P_2$	$C_{32}H_{40}Br_2MnN_6O_2P_2$	$C_{32}H_{40}I_2MnN_6O_2P_2$
Formula weight	744.48	817.40	911.38
Temperature	100(2) K	100(2) K	100(2) K
Wavelength	0.71073 Å	0.71073 Å	0.71073 Å
Crystal system	Monoclinic	Monoclinic	Triclinic
Space group	$P2_1/c$	$P2_1/c$	$P\text{-}1$
Unit cell dimensions	a = 13.4553(11) Å	a = 13.6104(12) Å	a = 13.5937(8) Å
	b = 7.5969(6) Å	b = 7.5925(8) Å	b = 16.1525(8) Å
	c = 33.633(3) Å	c = 33.857(4) Å	c = 18.1507(10) Å
	α = 90°	α = 90°	α = 70.450(2)°
	β = 94.306(3)°	β = 94.243(3)°	β = 78.827(2)°
	γ = 90°	γ = 90°	γ = 89.773(2)°
Volume	3428.2(5) Å^3	3489.1(6) Å^3	3676.5(4) Å^3
Z	4	4	4
Density (calculated)	1.442 Mg/m^3	1.556 Mg/m^3	1.647 Mg/m^3
Absorption coefficient	0.677 mm^{-1}	2.799 mm^{-1}	2.162 mm^{-1}
$F(000)$	1548	1660	1804
Crystal size	0.178 × 0.075 × 0.015 mm	0.213 × 0.092 × 0.015 mm	0.161 × 0.155 × 0.113 mm
Θrange for data collection	1.871 to 27.533°	1.854 to 28.316°	1.967 to 28.352°
Index ranges	$-17 < h \le 17$	$-18 \le h \le 14$	$-17 \le h \le 18$
	$-9 \le k \le 9$	$-10 \le k \le 10$	$-21 \le k \le 21$
	$-37 \le l \le 43$	$-45 \le l \le 45$	$-16 \le l \le 24$
Reflections collected	78,371	103,097	18,300
Independent reflections	7861 [R_{int} = 0.1080]	8659 [R_{int} = 0.0510]	18,300 [R_{int} = 0.0473]
Reflections observed (>2σ)	6716	7789	17,352
Data Completeness	0.996	0.997	0.997
Max. and min. transmission	0.7456 and 0.6371	0.7457 and 0.6192	0.7455 and 0.6771
Data / restraints / parameters	7861 / 0 / 423	8659 / 0 / 414	18,300 / 0 / 837
Goodness-of-fit on F^2	1.226	1.163	1.109
Final R indices [$I > 2\sigma(I)$]	R_1 = 0.1329	R_1 = 0.0389	R_1 = 0.0377
	wR_2 = 0.2880	wR_2 = 0.0830	wR_2 = 0.0948
R indices (all data)	R_1 = 0.1486	R_1 = 0.0450	R_1 = 0.0398
	wR_2 = 0.2947	wR_2 = 0.0851	wR_2 = 0.0960
Largest diff. peak and hole	3.282 and −1.639 e Å^{-3}	1.259 and −0.469 e Å^{-3}	4.223 and −1.842 e Å^{-3}

$[MnCl_2L_2]$. UV–VIS (CH_2Cl_2, 298 K, nm): <263, 280 sh, 288 (ε = 27800 M^{-1} cm^{-1}), 306, 320. PL (solid, r.t., $\lambda_{excitation}$ = 270 nm, nm): 396, 415, 441 ligands, 526 max $^4T_1(^4G) \rightarrow {}^6A_1(^6S)$, 546 sh, 595 sh, 649 sh ligands. PL (solid, r.t., $\lambda_{excitation}$ = 350 nm, nm): 396, 415, 441 ligands, 526 sh $^4T_1(^4G) \rightarrow {}^6A_1(^6S)$, 546 max, 558 sh, 595, 614 sh, 649 ligands. PLE (solid sample, r.t., $\lambda_{mission}$ = 520 nm, nm): <345 (max 265), 355, 370 ligands and $^4F,^4P,^4D \leftarrow {}^6A_1(^6S)$, 422, 438, 460 $^4G \leftarrow {}^6A_1(^6S)$. PLE (solid sample, r.t., $\lambda_{emission}$ = 650 nm, nm): <360 (max 349), 370 ligands and $^4F,^4P,^4D \leftarrow {}^6A_1(^6S)$, 422, 438, 460 $^4G \leftarrow {}^6A_1(^6S)$. τ_{obs} (solid sample, r.t., $\lambda_{excitation}$ = 290 nm, $\lambda_{emission}$ = 520 nm, μs): 305. Φ (solid, r.t., $\lambda_{excitation}$ = 365 nm): 5%.

$[MnBr_2L_2]$. UV–VIS (CH_2Cl_2, 298 K, nm): <263, 280 sh, 288 (ε = 28700 M^{-1} cm^{-1}), 306, 320. PL (solid, r.t., $\lambda_{excitation}$ = 270 nm, nm): 520 max $^4T_1(^4G) \rightarrow {}^6A_1(^6S)$, 625 ligands. PL (solid, r.t., $\lambda_{excitation}$ = 350 nm, nm): 520 $^4T_1(4G) \rightarrow {}^6A_1(^6S)$, 544 max, 593, 645 ligands. PLE (solid sample, r.t., $\lambda_{emission}$ = 520 nm, nm): <340 (max 321), 351, 370 ligands and $^4F,^4P,^4D \leftarrow {}^6A_1(^6S)$, 420, 441, 460 $^4G \leftarrow {}^6A_1(^6S)$. PLE (solid sample, r.t., $\lambda_{emission}$ = 650 nm, nm): <340 (max 321), 351, 370 ligands and $^4F,^4P,^4D \leftarrow {}^6A_1(^6S)$, 420, 441, 460 $^4G \leftarrow {}^6A_1(^6S)$. τ_{obs} (solid sample, r.t., $\lambda_{excitation}$ = 290 nm, $\lambda_{emission}$ = 520 nm, μs): 182. Φ (solid, r.t., $\lambda_{excitation}$ = 365 nm): 10%.

$[MnI_2L_2]$. UV–VIS (CH_2Cl_2, 298 K, nm): <263, 280 sh, 288 (ε = 26400 M^{-1} cm^{-1}), 306, 320. PL (solid, r.t., $\lambda_{excitation}$ = 270 nm, nm): 519 max $^4T_1(4G) \rightarrow {}^6A_1(^6S)$, 645 ligands. PL (solid, r.t., $\lambda_{excitation}$ = 350 nm, nm): 519 max $^4T_1(^4G) \rightarrow {}^6A_1(^6S)$, 645 ligands. PLE (solid sample, r.t., $\lambda_{emission}$ = 520 nm, nm): <340 (max 319), 340–395 ligands and $^4F,^4P,^4D \leftarrow {}^6A_1(^6S)$, 429, 446, 466 $^4G \leftarrow {}^6A_1(^6S)$. PLE (solid sample, r.t., $\lambda_{emission}$ = 650 nm, nm): <340 (max 319) ligands and $^4F \leftarrow {}^6A_1(^6S)$. τ_{obs} (solid sample, r.t., $\lambda_{excitation}$ = 290 nm, $\lambda_{emission}$ = 520 nm, μs): 71. Φ (solid, r.t., $\lambda_{excitation}$ = 365 nm): 5%.

2.5. Computational details

The computational geometry optimizations of $[MnX_2L_2]$ (X = Cl, Br, I) (quartet, sextet and octet states) were carried out without symmetry constraints, using the global-hybrid *meta*-NGA functional MN15 [58] and the def2 split-valence polarized basis set of Ahlrichs and Weigend, with ECP including 28 electrons for iodine [59]. The "unrestricted" formalism was applied and the absence of meaningful spin contamination was verified by comparing the computed $<S^2>$ value with the theoretical one [60]. The software used was Gaussian 16 [61]. Cartesian coordinates of the DFT-optimized structures are collected in a separated Supplementary data file.

3. Results and discussion

3.1. Synthesis and structural characterization of the complexes

The reaction of *N*,*N*,*N*′,*N*′-tetramethyl-*P*-carbazol-9-ylphosphonic diamide (L) with MnX_2 anhydrous halides (X = Cl, Br, I) in ethanol afforded complexes with general $[MnX_2L_2]$, as indicated by the elemental analysis data. The measured magnetic moments were in all the cases close to the 5.9 BM expected for high-spin d^5 metal complexes of the first transition series. No signal related to the free organic ligand was detected in the ^1H and $^{31}P\{^1H\}$ NMR spectra, as observable in Fig. S1. The ^1H NMR spectra show only broad signals related to the carbazolyl moiety, while the NMe_2 resonances are too relaxed to be easily distinguished. The $^{31}P\{^1H\}$ NMR resonance was observed as very broad singlet only in the case of **$[MnCl_2L_2]$**. Dichloromethane solutions of the complexes resulted not conductive. The IR spectra of the three $[MnX_2L_2]$ complexes are almost superimposable and similar to that of the free ligand. The coordination of L to Mn(II) halides causes a small shift to lower wavenumbers in the $\nu_{P\overline{\ }O}$ region, as highlighted in Fig. 1.

The general formulation of the three complexes was confirmed by single-crystal X-ray diffraction. In all the compounds the Mn(II) ion is coordinated by two halogen atoms and two oxygen atoms of two *N*,*N*,*N*′,*N*′-tetramethyl-*P*-carbazol-9-ylphosphonic diamide ligands. The structures of **$[MnBr_2L_2]$** and **$[MnI_2L_2]$** are shown in Fig. 2. Selected bond lengths and angles are collected in Table 2.

$[MnCl_2L_2]$ and **$[MnBr_2L_2]$** are isomorphs and crystallize in the monoclinic $P2_1/c$ space group. It should be noted that data of **$[MnCl_2L_2]$** are of scarce quality (see the Experimental Section), so its geometrical parameters should be read with caution. **$[MnI_2L_2]$** crystallizes in the triclinic *P*-1 space group and contains two molecules in the asymmetric unit, with scarce differences between them. One of them is shown in Fig. 2. **$[MnI_2L_2]$** exhibits some differences with respect to the other two compounds, as highlighted by the superimposition of **$[MnBr_2L_2]$** and **$[MnI_2L_2]$** in Fig. 3. The variation of the Mn–X bonds follows the expected sequence Mn-Cl < Mn-Br < Mn-I, and the average Mn–O bond length becomes shorter on increasing the Mn-X distance. The environment around Mn(II) is best described as a slightly distorted tetrahedron, as occurs for other $[MnX_2(phosphoramide)_2]$ complexes [38,42,44], with τ_4 [64] or τ'_4 [65] around 0.92 ($\tau_4 = 0$ for square planar, $\tau_4 = 1$ for tetrahedral). The angles around Mn(II) are comprised between 95.2(3) and 121.02(2)°. In the complexes here reported the X-Mn-X angles are not the most obtuse, as instead occurs for the related indol-1-yl derivatives [44], being one of the X-Mn-O angles slightly bigger. A similar situation was however observed for Mn(II) halide complexes with 1,3-dimethyl-2-phenyl-1,3-diazaphospholidine-2-oxide as ligand [43]. The lower angle always corresponds to the O-Mn-O one, and decreases passing from **$[MnI_2L_2]$** to **$[MnCl_2L_2]$**. The values, between 95.2(3) and 97.92(10)°, are very far from the ideal 109.5° probably because of the sterical hindrance of the carbazolyl-based ligand. It is worth noting that in the *N*,*N*,*N*′,*N*′-tetramethyl-*P*-indol-1-ylphosphonic diamide complexes [44] the O-Mn-O angles are close to the expected value for a tetrahedron, being comprised between 104.88 (6) and 106.80(9)°. In addition, other peculiar differences with respect to other phosphoramide-based Mn(II) complexes are observable. For instance, Figg. 2 and 3 show changes in the orientation of the carbazolyl moieties on changing the coordinated halide. In **$[MnCl_2L_2]$** and **$[MnBr_2L_2]$** the dihedral angles between the best planes are respectively 80.26(9) and 79.33(3)°, while the values for the same angle in **$[MnI_2L_2]$** are 16.37(10) and 8.92(9)° for the two molecules in the asymmetric unit. The planes are therefore almost perpendicular in **$[MnCl_2L_2]$** and **$[MnBr_2L_2]$** and roughly parallel in **$[MnI_2L_2]$**. For comparison, the same dihedral angles in the *N*,*N*,*N*′,*N*′-tetramethyl-*P*-indol-1-ylphosphonic diamide complexes have intermediate values, 63.5(1), 63.14(6) and 62.19(7)°, very similar on changing the halide with a slight increase

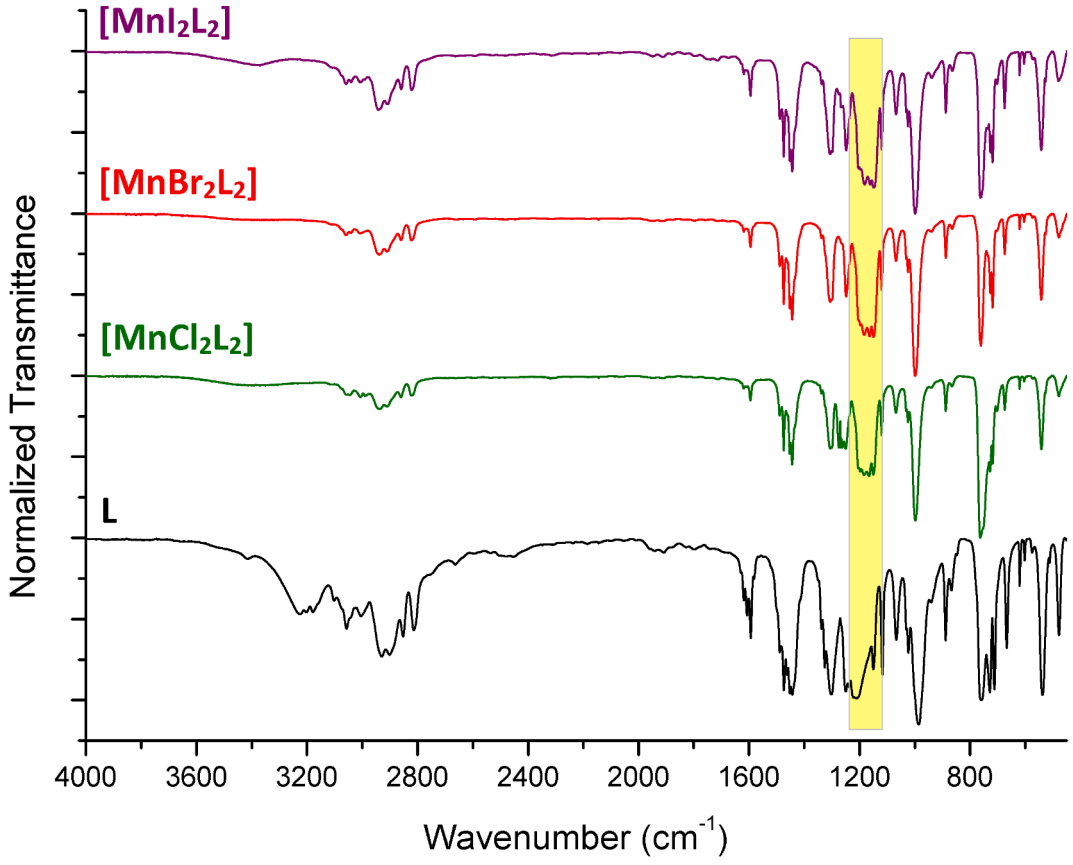

Fig. 1. IR spectra of L and of the $[MnX_2L_2]$ complexes (X = Cl, Br, I).

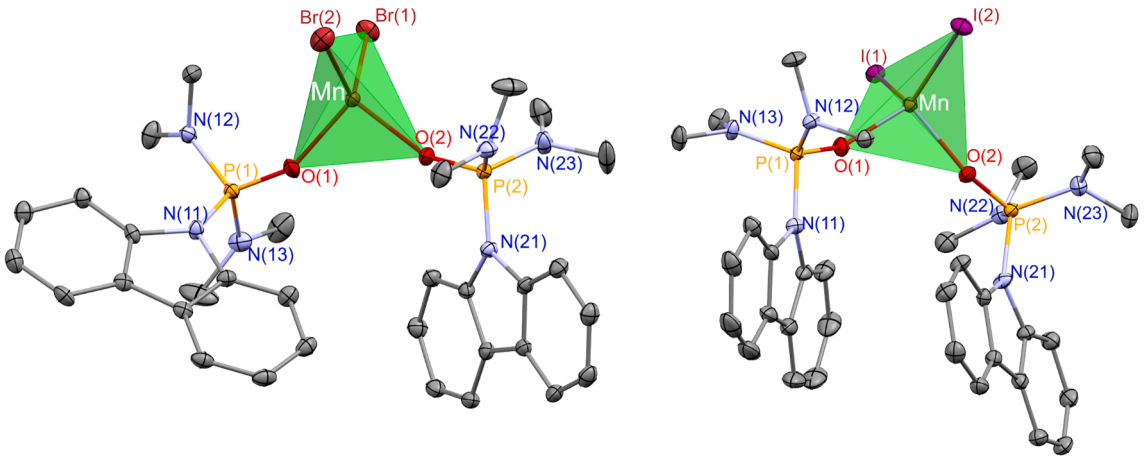

Fig. 2. X-ray structures of the $[MnX_2L_2]$ complexes (X = Br, I) [62,63].

Table 2
Selected bond lengths [Å] and angles [°] for MnX_2L_2 complexes (X = Cl, Br, I).

	[$MnCl_2L_2$] *	**[$MnBr_2L_2$]**	**[MnI_2L_2]** (1st molecule)	**[MnI_2L_2]** (2nd molecule)
Mn-O(1)	2.047(6)	2.042(2)	2.033(2)	2.035(3)
Mn-O(2)	2.035(6)	2.0423(19)	2.037(2)	2.041(3)
Mn-X(1)	2.329(3)	2.4748(5)	2.6644(6)	2.6761(6)
Mn-X(2)	2.340(3)	2.4619(6)	2.6843(6)	2.6857(6)
O(1)-P(1)	1.485(6)	1.484(2)	1.493(3)	1.492(3)
P(1)-N(11)	1.688(7)	1.680(2)	1.692(3)	1.687(3)
P(1)-N(12)	1.620(8)	1.616(2)	1.618(3)	1.618(3)
P(1)-N(13)	1.627(7)	1.619(2)	1.626(3)	1.624(3)
P(2)-O(2)	1.498(6)	1.4874(19)	1.489(3)	1.492(3)
P(2)-N(21)	1.689(7)	1.694(2)	1.692(3)	1.691(3)
P(2)-N(22)	1.616(8)	1.616(2)	1.622(3)	1.615(3)
P(2)-N(23)	1.616(7)	1.621(2)	1.630(3)	1.631(3)
O(2)-Mn-O(1)	95.2(3)	95.79(8)	97.92(10)	96.92(10)
O(2)-Mn-X(1)	112.5(2)	112.65(6)	111.67(7)	106.02(8)
O(2)-Mn-X(2)	112.2(2)	113.12(6)	105.09(7)	116.61(7)
O(1)-Mn-X(1)	113.5(2)	109.78(6)	108.31(7)	110.24(7)
O(1)-Mn-X(2)	109.3(2)	113.39(7)	110.32(7)	109.65(7)
X(1)-Mn-X(2)	112.92(10)	111.244(18)	121.02(2)	115.58(2)
P(1)-O(1)-Mn	151.6(4)	152.31(13)	118.12(15)	109.98(16)
P(2)-O(2)-Mn	151.2(4)	149.79(13)	148.89(16)	150.95(17)

* Data of this crystal have low quality (as evidenced by the high e.s.d. in parenthesis), but values with low accuracy are included here for comparison with the other compounds.

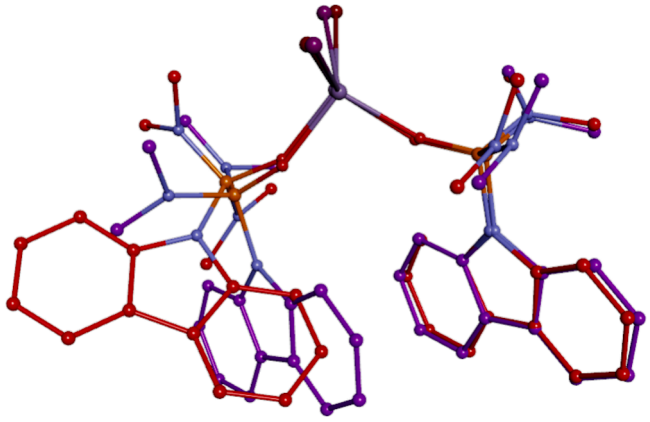

Fig. 3. Superimposition of **[$MnBr_2L_2$]** (carbon atoms in red) and **[MnI_2L_2]** (carbon atoms in violet). **[$MnCl_2L_2$]** is not depicted because it is isomorph to **[$MnBr_2L_2$]** and its crystal structure has low quality.

following the order X = I < X = Br < X = Cl. The Mn-O-P angles are around 145-150° in most of the $[MnX_2(phosphoramide)_2]$ complexes previously described, with values up to 170° in selected cases [42,44]. To the best of our knowledge [66] the behaviour of **[MnI_2L_2]** is surprising, because one of the two *N,N,N′,N′*-tetramethyl-*P*-carbazol-9-ylphosphonic diamide ligands is definitively bent, with values for the angle of 118.12(15) and 109.98(16)°. The other ligand shows expected values, equal to 148.89(16) and 150.95(17)°.

The computational geometry optimizations of the $[MnX_2L_2]$ complexes at the sextet ground state, carried out *in vacuo*, afforded stationary points with $\{MnX_2O_2\}$ first coordination spheres strictly comparable to the experimental data (molecular overlay values: 99.7% for X = Cl and X = Br, 99.9% and 99.7% for X = I, depending upon the choice of the molecule in the asymmetric unit). The superimpositions are shown in Fig. S2 and experimental and computed bond lengths are compared in Table S1. On considering the entire molecules, the overly values are 78.5% for **[$MnCl_2L_2$]**, 84.5% for **[$MnBr_2L_2$]** and between 97.9% and 98.9% for **[MnI_2L_2]**. The main differences are related to the spatial disposition of the substituents on the phosphoramide ligands, probably attributable to the lack of packing forces affecting the DFT-optimized structures.

3.2. *Photoluminescence of the complexes*

The $[MnX_2L_2]$ complexes have superimposable absorption spectra in CH_2Cl_2 solution, with a peak in the UV region at 288 nm (absorption coefficient around 28000 M^{-1} cm^{-1}). The spectra are strictly comparable to that of the free ligand, as observable in Fig. S3. The complexes do not show appreciable photoluminescence in solution, but bright emission in the visible range is observable upon excitation of solid samples with UV light. Unfortunately, no triboluminescence could be detected. All the photoluminescence measurements were carried out on freshly prepared samples before and after crystallization, and no appreciable change was observed. The absorption of the solid complexes in the UV range was confirmed by reflectance measurements (see for instance Fig. S4). The instrument used allowed the simultaneous irradiation and collection of light in the 220–1000 nm range, therefore the superimposition of the absorption and emission of the samples was observed.

The photoluminescence of **[$MnCl_2L_2$]** shows meaningful changes on varying the excitation wavelength, as observable in Fig. 4a. The spectra obtained for short excitation wavelengths (see for instance the PL spectrum obtained for $\lambda_{excitation}$ = 270 nm, Fig. 4b) are dominated by a band centred at 526 nm, attributable to the Mn(II) $^4T_1(^4G) \rightarrow {}^6A_1(^6S)$ transition. Further bands are present for wavelengths below 450 nm and in the red region of the spectrum. The relative intensity of the bands is

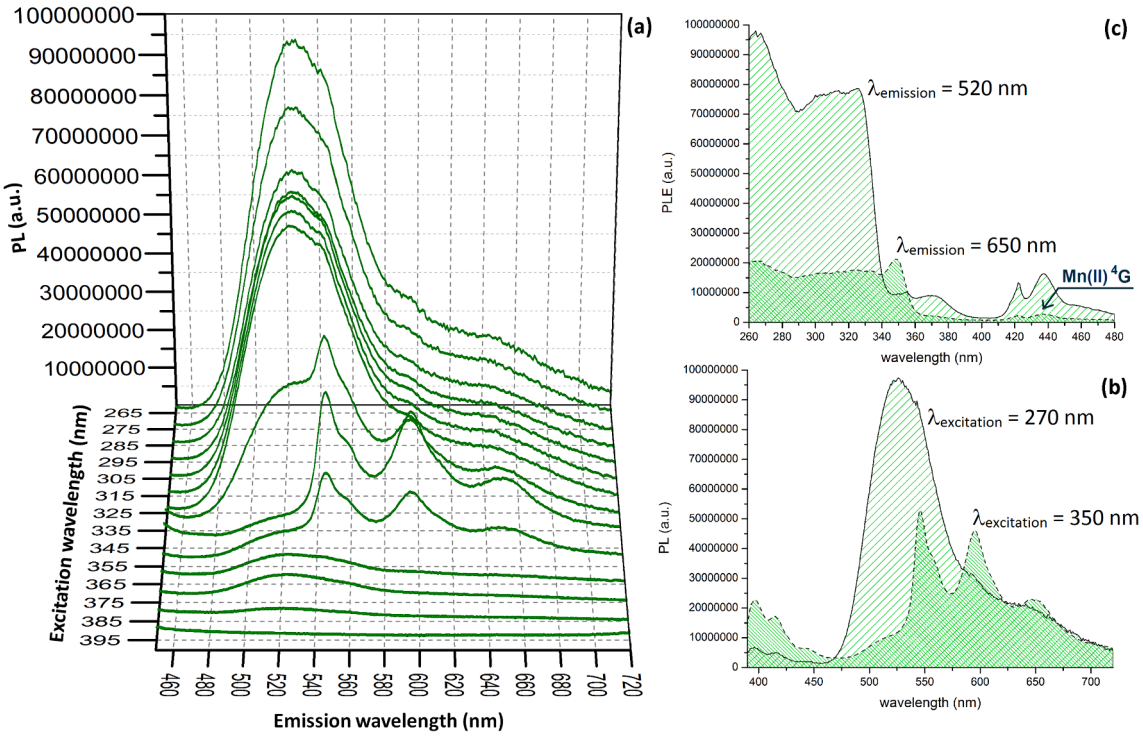

Fig. 4. (a) PL spectra of **[$MnCl_2L_2$]** at different excitation wavelengths. (b) PL spectra of **[$MnCl_2L_2$]** for $\lambda_{excitation} = 270$ nm and $\lambda_{excitation} = 350$ nm. (c) PLE spectra of **[$MnCl_2L_2$]** for $\lambda_{emission} = 520$ nm and $\lambda_{emission} = 650$ nm. Solid sample, r.t.

very different in the spectrum recorded for $\lambda_{excitation} = 350$ nm (Fig. 4b), where the Mn(II)-centred transition is weaker than the bands at lower wavelengths. Such a behaviour agrees with the different PLE spectra obtained for emission at 520 and 650 nm (Fig. 4c). Both the spectra show three bands between 410 and 480 nm attributable to the excitation from $^6A_1(^6S)$ to the ^4G manifold, separated in three sublevels by the tetrahedral field surrounding Mn(II). This evidence, highlighted in Fig. 4c, indicates that the emission either in the green and in the red region is somewhat related to the Mn(II) ^4G state. The PLE bands at wavelengths below 400 nm are attributable to both Mn(II) and ligands excitation, the latter prevailing in the PLE spectrum recorded for $\lambda_{excitation} = 650$ nm. The different PLE spectra on changing the excitation wavelength allow to suppose that the emission in the red range could be associated to excited states of the coordinated ligands. It is therefore likely to propose that the emission of **[$MnCl_2L_2$]** is composed by the superimposition of metal- and ligand-centred transitions, in line with the results obtained for related *N,N,N′,N′*-tetramethyl-*P*-naphtalen-2-ylphosphonic diamide Mn(II) halide complexes [45]. Such a superimposition was already observed for the Eu(III) nitrato-complex of *N,N,N′,N′*-tetramethyl-*P*-carbazol-9-ylphosphonic diamide [50].

The PL spectrum of the free ligand (Fig. S5) shows transitions in the blue-violet region and broad bands in the 450–600 nm range. It is worth noting that the luminescence lifetime obtained for the free ligand (solid sample, r.t., $\lambda_{emission} = 520$ nm) is 15 ns (Fig. S5), in line with emission from excited singlet states. On comparing the spectra, the emission bands at wavelengths below 400 nm observed for **[$MnCl_2L_2$]** (Fig. 4b) are attributable to weak luminescence from the excited singlet state of the coordinated ligands. On the other hand, the transitions at longer wavelengths fall at lower energy with respect to the free ligand and can be tentatively attributed to the population of an excited state with different multiplicity.

It is worth noting that the Racah *B* parameter obtained from the wavelength of the $(^4A_1+^4E)^4G \leftarrow {}^6A_1(^6S)$ transition is around 730 cm^{-1} (nephelauxetic ratio around 0.79 [67]), strictly comparable to other Mn (II) tetrahedral complexes with similar first coordination sphere [40].

The possibility of impurities at the basis of the dual emission of **[$MnCl_2L_2$]** was definitely ruled out studying the luminescence decay curves of the crystallized sample at different emission wavelengths. As observable in the semi-log plot reported in Fig. 5, after excitation at 290 nm the luminescence decay curves obtained for $\lambda_{emission} = 520$ nm and $\lambda_{emission} = 700$ nm are roughly parallel in the 700–2000 μs range, in agreement with only one species causing the photoluminescent behaviour. From the PL decay collected at $\lambda_{emission} = 520$ nm the observed lifetime τ_{obs} of the $^4T_1(^4G)$ level is estimated around 305 μs. The time shift of the curve for $\lambda_{emission} = 700$ nm suggests that a different emitting level, most likely ligand-centred (LC), is populated by the $^4T_1(^4G)$ excited state and that the lifetime of the energy transfer is in the μs range. The parallel decays observed for $\lambda_{emission} = 700$ nm and $\lambda_{emission} = 520$ nm also indicate that the lifetime of the lowest energy excited state is longer than that of the $^4T_1(^4G)$ one. The emission of **[$MnCl_2L_2$]** can be compared to a dual phosphorescence [68,69], a phenomenon recently reported for instance for biscarbazole and dibenzothiophene derivatives [70–72]. In principle, if a molecule could decay radiatively from two excited states with different multiplicity with respect to the ground state, the chance to observe non-Kasha dual emission occurs in two ways: the former is based on large energy separation between the two states and relatively fast decay from the highest energy level, while the latter requires that the two excited states have a small energy gap and are thermally equilibrated. The dual luminescence of **[$MnCl_2L_2$]** appears in line with the first scenario, while the second one was suggested for the previously mentioned aromatic compounds.

The proposed description of the photoluminescence was partially supported by the simplified numerical simulation of the decay curves, shown in Fig. 5. Starting from the experimental curve describing the LED pulse used for excitation [EX], the population of the first emitting state over time [P1] was calculated accordingly to Eqn. (1), where τ_1 describes the decay of [P1] to the ground state and τ_2 the energy transfer to the second emitting state, [P2]. Consequently, the population [P2] over time depends on [P1] owing to Eqn. (2), if back energy transfer from [P2] to [P1] is neglected. The possible direct population of [P2] from [EX] was not considered for simplicity. The constant τ_3 accounts for the decay of [P2] to the ground state. Finally, the observed lifetime τ_{obs}

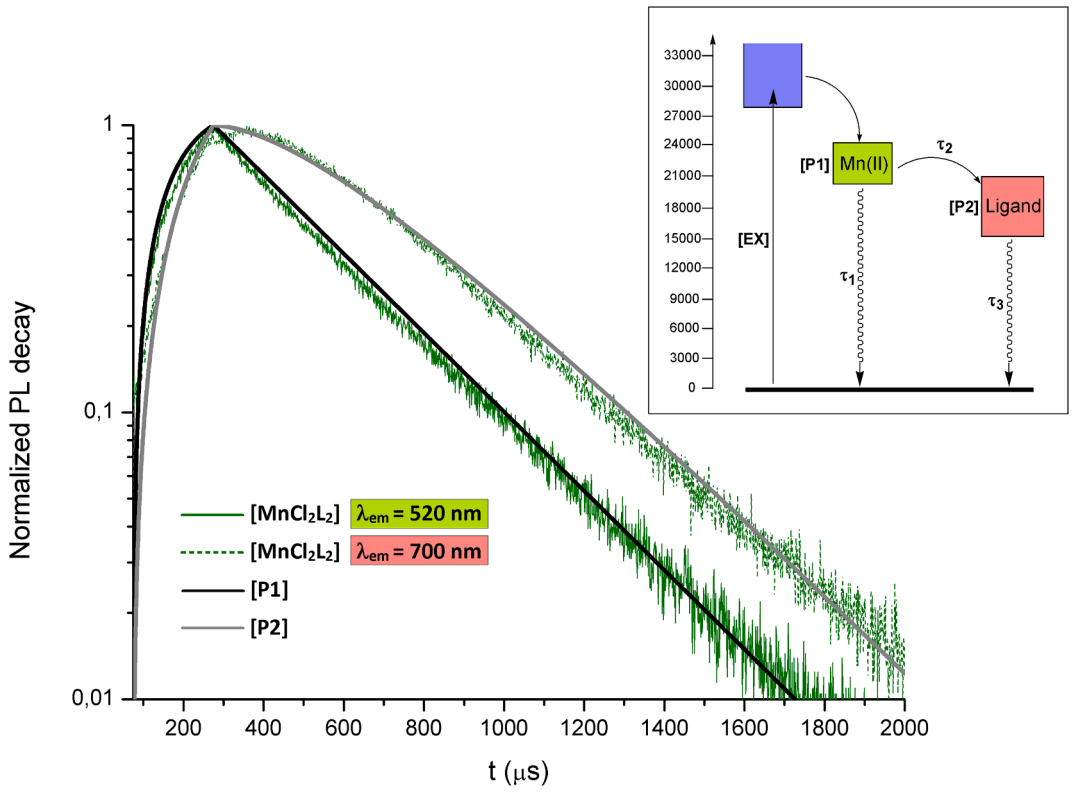

Fig. 5. Semi-log plot of the luminescence decay curves of **[$MnCl_2L_2$]** (solid sample, r.t., $\lambda_{excitation}$ = 290 nm). Inset: model used to simulate the luminescence decay curves.

should be related to τ_1 and τ_2 on the basis of Eqn. (3). The model used is sketched in the inset of Fig. 5 for clarity.

$$[P1] = [EX]e^{-t(\frac{1}{\tau_1}+\frac{1}{\tau_2})} \quad (1)$$

$$[P2] = ([P1](1 - e^{-t(\frac{1}{\tau_2})}))e^{-t(\frac{1}{\tau_3})} \quad (2)$$

$$\frac{1}{\tau_{obs}} = \frac{1}{\tau_1} + \frac{1}{\tau_2} \quad (3)$$

Despite not conclusive, the simulation in Fig. 5 appears acceptable, being τ_1 and τ_2 values in the hundreds of μs range (abut 550 and 700 μs, respectively) and τ_3 almost one order of magnitude greater.

The possible role of the carbazolyl groups in the luminescence of **[$MnCl_2L_2$]** was also suggested by the comparison of the spin density plots of **[$MnCl_2L_2$]** optimized at the sextet ground state and at the lowest energy octet state (Fig. S6). The spin density related to the two new unpaired electrons is fully localized on one of the carbazolyl substituents, accordingly to the hypothesis of an emitting level having LC nature.

As for **[$MnCl_2L_2$]**, the PL spectra of **[$MnBr_2L_2$]** and **[MnI_2L_2]** show dual emission attributable to $^4T_1(^4G)$ and LC decays, but the wavelength-dependent behaviour is less evident for **[$MnBr_2L_2$]** and negligible for **[MnI_2L_2]**, in line with PLE spectra affected to a lesser extent by the emission wavelength (Fig. 6). The presence of the Mn(II) $^4T_1(^4G) \leftarrow {}^6A_1(^6S)$ transitions also in the PLE spectra recorded for $\lambda_{emission}$ = 650 nm indicates the possibility of energy transfer from Mn (II) excited states to the lowest energy emitting level, as previously described for **[$MnCl_2L_2$]** (Fig. 6).

The ratio between Mn(II) and ligands excitation bands is reduced in **[$MnBr_2L_2$]** and **[MnI_2L_2]** with respect to **[$MnCl_2L_2$]**. To shed light into the changes observed on varying the coordinated halides, the increased spin–orbit coupling moving from X = Cl to X = I must be considered [73]. The different processes that can be variably affected by the choice of the halide are summarized in Scheme 1 for clarity. It is reasonable to suppose that the increased spin–orbit coupling accelerates in particular the processes involving Mn(II)-centred states, more strictly coupled with the halides with respect to those of the [O=P]-donor ligands. On the basis of this assumption, the energy transfer to Mn(II) after the excitation of the coordinated ligands, **(b)** in Scheme 1, is accelerated with respect to the radiative decay from the ligand **(a)** and the intersystem crossing **(c)** between ligand-centred states. Accordingly, the luminescence at higher wavelengths disappears in the PL spectra of **[$MnBr_2L_2$]** and **[MnI_2L_2]** (Fig. S7). The lack of important excitation-dependent behaviour in **[$MnBr_2L_2$]** and **[MnI_2L_2]** can be explained on the basis of the reduced relative importance of the process **(c)**. Moreover, the radiative decay from the Mn(II) emitting state, **(d)** in Scheme 1, is accelerated with respect to the decay from the ligands **(f)**, accordingly to PL spectra with growing relative intensity of the $^4T_1(^4G) \rightarrow {}^6A_1(^6S)$ transition on increasing the atomic number of the coordinated halides (Fig. S7). Another process accelerated by the spin–orbit coupling is the energy transfer from Mn(II) to the emitting state at lower energy, **(e)** in Scheme 1, perhaps at the basis of the dual emission observed also for **[$MnBr_2L_2$]** and **[MnI_2L_2]**.

The luminescence decay curves of **[$MnBr_2L_2$]** and **[MnI_2L_2]** in Fig. 7 confirm the time shift of the PL decay curve collected for $\lambda_{emission}$ = 700 nm, in agreement with a mechanism strictly comparable to that proposed for **[$MnCl_2L_2$]**. The replacement of chloride with heavier halides causes the expected reduction of the τ_{obs} values [73], respectively 182 and 71 μs for **[$MnBr_2L_2$]** and **[MnI_2L_2]** ($\lambda_{emission}$ = 520 nm). The lifetime values of the three complexes are summarized in Table 3 for clarity.

Further measurements revealed that the decay curves of the three $[MnX_2L_2]$ complexes collected at $\lambda_{emission}$ = 700 nm are bi-exponential, while those recorded at $\lambda_{emission}$ = 520 nm are mono-exponential. The second lifetimes are much longer (thousands of μs range) than the τ_{obs} values at $\lambda_{emission}$ = 520 nm, compatibly with the mechanism proposed for the dual luminescence and corresponding to the process **(f)** in

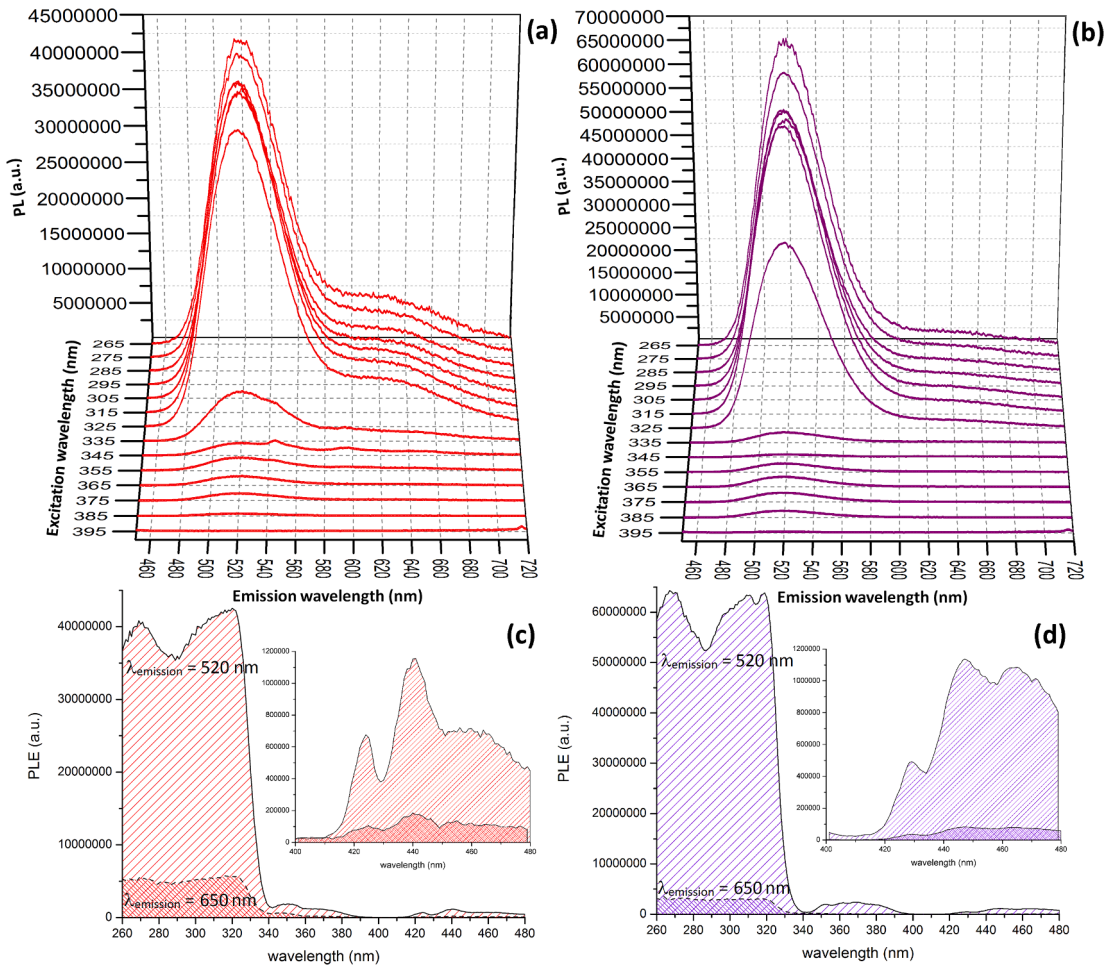

Fig. 6. (a) PL spectra of **[MnBr$_2$L$_2$]** at different excitation wavelengths. (b) PL spectra of **[MnI$_2$L$_2$]** at different excitation wavelengths. (c) PLE spectra of **[MnBr$_2$L$_2$]** for $\lambda_{emission}$ = 520 nm and $\lambda_{emission}$ = 650 nm. (d) PLE spectra of **[MnI$_2$L$_2$]** for $\lambda_{emission}$ = 520 nm and $\lambda_{emission}$ = 650 nm. Solid samples, r.t.

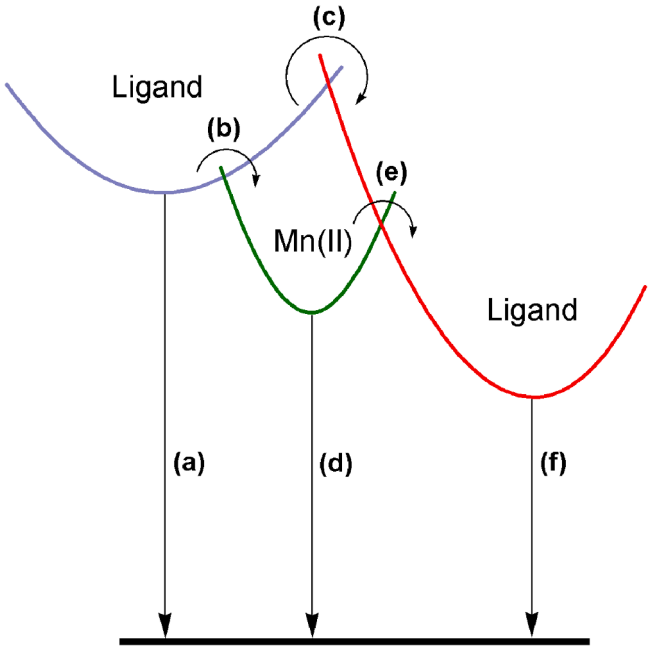

Scheme 1. Simplified description of the energy transfer processes in [MnX$_2$L$_2$] complexes.

Scheme 1. Unfortunately, the decay curves do not allow a precise determination of the lifetime values for the slower process (see for instance the inset of Fig. 7 related to **[MnI$_2$L$_2$]**).

The photoluminescence quantum yields of the [MnX$_2$L$_2$] complexes are comprised between 5% and 10% (Table 3), roughly in line with previous measurements on tetrahedral Mn(II) halide complexes with *N*, *N*,*N*′,*N*′-tetramethyl-*P*-naphtalen-2-ylphosphonic diamide [45] and lower than that measured for [MnBr$_2$(*N*,*N*,*N*′,*N*′-tetramethyl-*P*-indol-1-ylphosphonic diamide)$_2$] [44], confirming that the introduction of π-conjugated substituents with accessible low-energy excited states favours non-radiative decay routes. The vibrational decay is also related to the distortion of the Mn(II) first coordination sphere from the sextet ground state to the excited quartet state, that was simulated for **[MnCl$_2$L$_2$]** by means of DFT calculations. The RMSD between the computed geometries is 1.187 Å, that becomes 0.768 Å on considering the {MnCl$_2$O$_2$} fragment. The superimposition shown in Fig. S8 highlights the tetragonal distortion of the first coordination sphere at the quartet state.

Given the presence of two correlated emissions in the PL spectra of the [MnX$_2$L$_2$] complexes, the correlation between lifetimes and quantum yields is not straightforward. By simply applying the equation $\Phi = k^r/(k^r + k^{nr})$ [74] (k^r = radiative rate constant, k^{nr} = non-radiative rate constant) with the replacement of $(k^r + k^{nr})^{-1}$ with the τ_{obs} values ($\lambda_{emission}$ = 520 nm), the k^r values thus obtained follow a roughly linear growth with the atomic number of the halide, underlining once more the paramount importance of spin–orbit coupling in this family of compounds (Table 3).

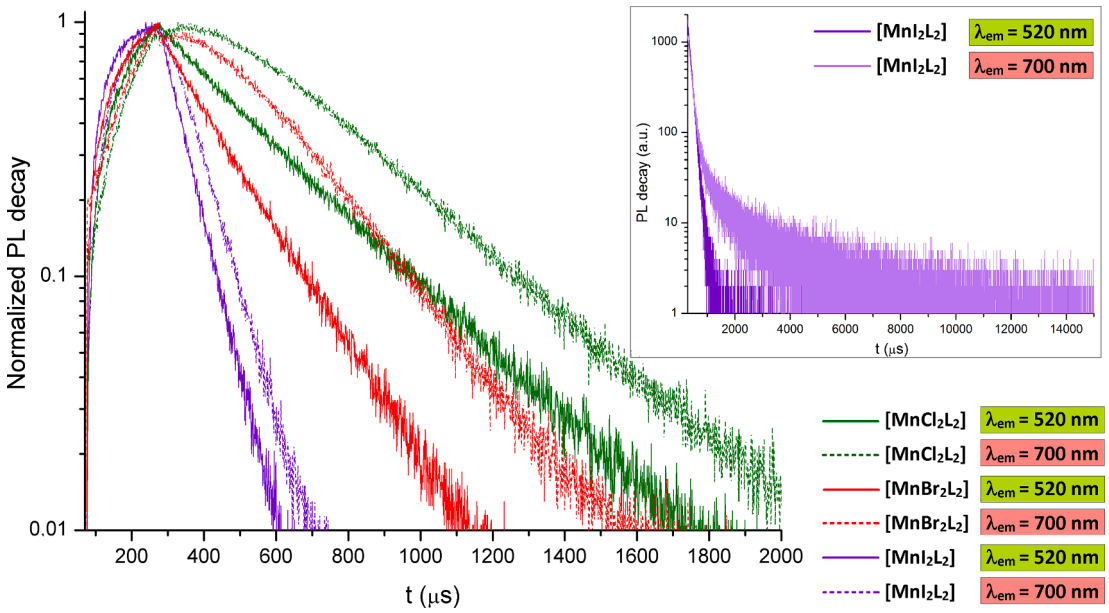

Fig. 7. Normalized luminescence decay curves of the $[MnX_2L_2]$ complexes (solid samples, r.t., $\lambda_{excitation} = 290$ nm). Inset: Semi-log plot of the luminescence decays curves of **$[MnI_2L_2]$** (solid sample, r.t., $\lambda_{excitation} = 290$ nm): violet line ($\lambda_{emission} = 520$ nm), lilac line ($\lambda_{emission} = 700$ nm).

Table 3
τ_{obs} and Φvalues, estimated radiative rate constants k^r and their dependence upon the atomic number Z of the coordinated halides.

	τ_{obs}[a] (μs)	Φ (%)[b]	k^r (s^{-1})	Z halide
$[MnCl_2L_2]$	305	5	$1.6 \cdot 10^2$	17
$[MnBr_2L_2]$	182	10	$5.5 \cdot 10^2$	36
$[MnI_2L_2]$	71	5	$7.0 \cdot 10^2$	53

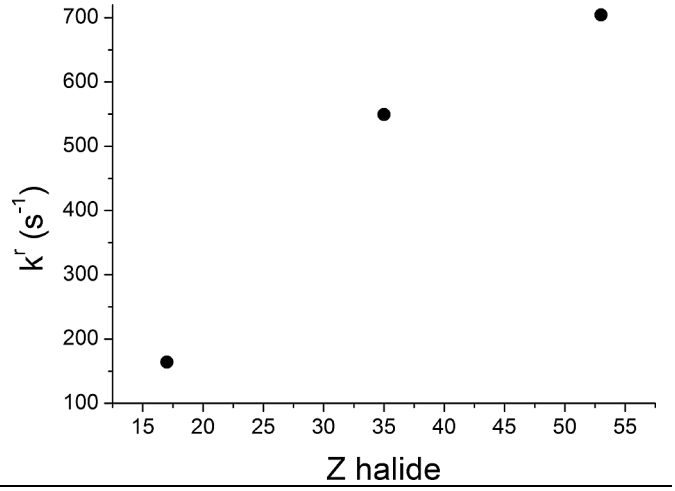

[a]$\lambda_{excitation} = 290$ nm, $\lambda_{emission} = 520$ nm. [b]$\lambda_{excitation} = 365$ nm.

4. Conclusions

The comparison of the results provided in this work with previous outcomes on similar tetrahedral Mn(II) complexes highlights that small changes in the electronic structure of the ligands strongly alter the photoluminescence of the complexes. The behaviour of *N*,*N*,*N*′,*N*′-tetramethyl-*P*-carbazol-9-ylphosphonic diamide complexes is different with respect to arylphosphonic diamide derivatives with phenyl or indol-1-yl substituents, that showed only green emission from the Mn(II) $^4T_1(^4G)$ excited state. The behaviour of the new compounds is more comparable to that of *N*,*N*,*N*′,*N*′-tetramethyl-*P*-naphtalen-2-ylphosphonic diamide complexes, where the superimposition of two different emission bands was observed, tentatively attributed to radiative decays from communicating metal- and ligand-centred excited states. Such a hypothesis is proposed also for the *N*,*N*,*N*′,*N*′-tetramethyl-*P*-carbazol-9-ylphosphonic diamide Mn(II) derivatives, and it is supported by the luminescence decay curves collected at different emission wavelengths. It is worth noting that the emission of the **$[MnCl_2L_2]$** complex is clearly wavelength-dependent, a feature of potential interest in optics and lighting technology that deserves further insight, also on considering possible different functionalizations of the phosphoramide skeleton.

Declaration of Competing Interest

The authors declare that they have no known competing financial interests or personal relationships that could have appeared to influence the work reported in this paper.

Acknowledgements

Università Ca' Foscari Venezia is gratefully acknowledged for financial support (Bando Spin 2018, D. R. 1065/2018 prot. 67416).

CACTI (University of Vigo) is gratefully acknowledged for X-ray data collection. CINECA (Bologna) is gratefully acknowledged for hardware and software availability (COLUMN21 project). We sincerely thank Prof. Massimo Sgarzi, Università Ca' Foscari Venezia, for the fruitful discussions.

Appendix A. Supplementary data

Supplementary data to this article can be found online at https://doi.org/10.1016/j.ica.2022.120896.

References

[1] S. Balsamy, P. Natarajan, R. Vedalakshmi, S. Muralidharan, Triboluminescence and vapor-induced phase transitions in the solids of methyltriphenylphosphonium tetrahalomanganate(II) complexes, Inorg. Chem. 53 (12) (2014) 6054–6059.

[2] C. Jiang, N. Zhong, C. Luo, H. Lin, Y. Zhang, H. Peng, C.-G. Duan, (Diisopropylammonium)$_2$MnBr 4: a multifunctional ferroelectric with efficient green-emission and excellent gas sensing properties, Chem. Commun. 53 (2017) 5954–5957.

[3] L.-J. Xu, C.-Z. Sun, H. Xiao, Y. Wu, Z.-N. Chen, Green-light-emitting diodes based on tetrabromide manganese(II) complex through solution process, Adv. Mater. 29 (2017) 1605739.

[4] S. Chen, J. Gao, J. Chang, Y. Zhang, L. Feng, Organic-inorganic manganese (II) halide hybrids based paper sensor for the fluorometric determination of pesticide ferbam, Sens. Actuators B 297 (2019), 126701.

[5] J. Zhao, T. Zhang, X.-Y. Dong, M.-E. Sun, C. Zhang, X. Li, Y.S. Zhao, S.-Q. Zang, Circularly polarized luminescence from achiral single crystals of hybrid manganese halides, J. Am. Chem. Soc. 141 (40) (2019) 15755–15760.

[6] L. Mao, P. Guo, S. Wang, A.K. Cheetham, R. Seshadri, Design principles for enhancing photoluminescence quantum yield in hybrid manganese bromides, J. Am. Chem. Soc. 142 (31) (2020) 13582–13589.

[7] L.-J. Xu, X. Lin, Q. He, M. Worku, B. Ma, Highly efficient eco-friendly X-ray scintillators based on an organic manganese halide, Nat. Commun. 11 (2020) 4329.

[8] Y.i. Zhang, W.-Q. Liao, D.-W. Fu, H.-Y. Ye, C.-M. Liu, Z.-N. Chen, R.-G. Xiong, The first organic-inorganic hybrid luminescent multiferroic: (pyrrolidinium)MnBr 3, Adv. Mater. 27 (26) (2015) 3942–3946.

[9] Y. Zhang, W.-Q. Liao, D.-W. Fu, H.-Y. Ye, Z.-N. Chen, R.-G. Xiong, Highly efficient red-light emission in an organic-inorganic hybrid ferroelectric: (pyrrolidinium) $MnCl_3$, J. Am. Chem. Soc. 137 (15) (2015) 4928–4931.

[10] H.-Y. Ye, Q. Zhou, X. Niu, W.-Q. Liao, D.-W. Fu, Y.i. Zhang, Y.-M. You, J. Wang, Z.-N. Chen, R.-G. Xiong, High-temperature ferroelectricity and photoluminescence in a hybrid organic-inorganic compound: (3-Pyrrolinium)$MnCl_3$, J. Am. Chem. Soc. 137 (40) (2015) 13148–13154.

[11] Y.-M. You, W.-Q. Liao, D. Zhao, H.-Y. Ye, Y. Zhang, Q. Zhou, X. Niu, J. Wang, P.-F. Li, D.-W. Fu, Z. Wang, S. Gao, K. Yang, J.-M. Liu, J. Li, Y. Yan, R.-G. Xiong, An organic-inorganic perovskite ferroelectric with large piezoelectric response, Science 357 (6348) (2017) 306–309.

[12] X. Liu, C. Ge, Z. Yang, Y. Song, A. Wang, Y. Kang, B. Li, Q. Dong, Guanidine-templated manganese halides single crystals toward efficient mechanoluminescence and photoluminescence by supramolecular interactions modulation, Adv. Opt. Mater. 9 (2021) 2100862.

[13] A.S. Berezin, A halomanganates(II) with P, P'-diprotonated bis(2-diphenylphosphinophenyl)ether: wavelength-excitation dependence of the quantum yield and role of the non-covalent interactions, Int. J. Mol. Sci. 22 (2021) 6873.

[14] A.S. Berezin, A brightly emissive halomanganates(II) with triphenylphosphonium cation: Synthesis, luminescence, and up-conversion phenomena, Dyes Pigments 196 (2021), 109782.

[15] S. Zhang, Y. Zhao, J. Zhou, H. Ming, C.-H. Wang, X. Jing, S. Ye, Q. Zhang, Structural design enables highly-efficient green emission with preferable blue light excitation from zero-dimensional manganese(II) hybrids, Chem. Eng. J. 421 (2021), 129886.

[16] S. Zhang, Y. Zhao, Y. Zhou, M. Li, W. Wang, H. Ming, X. Jing, S. Ye, Dipole-Orientation-dependent Förster resonance energy transfer from aromatic head groups to $MnBr_4^{2-}$ – blocks in organic-inorganic hybrids, J. Phys. Chem. Lett. 12 (36) (2021) 8692–8698.

[17] A. Jana, V. Gopalan Sree, Q. Ba, S. Chan Cho, S. Uck Lee, S. Cho, Y. Jo, A. Meena, H. Kim, H. Im, Efficient organic manganese(II) bromide green-light-emitting diodes enabled by manipulating the hole and electron transport layer, J. Mater. Chem. C 9 (2021) 11314–11323.

[18] S. Wang, X. Han, T. Kou, Y. Zhou, Y. Liang, Z. Wu, J. Huang, T. Chang, C. Peng, Q. Wei, B. Zou, Lead-free Mn^{II}-based red-emitting hybrid halide $(CH_6N_3)_2MnCl_4$ toward high performance warm WLEDs, J. Mater. Chem. C 9 (14) (2021) 4895–4902.

[19] P. Fu, Y. Sun, Z. Xia, Z. Xiao, Photoluminescence behavior of zero-dimensional manganese halide tetrahedra embedded in conjugated organic matrices, J. Phys. Chem. Lett. 12 (31) (2021) 7394–7399.

[20] J. He, H. Zhao, X. Hu, Z. Fangg, J. Wang, R. Zhang, G. Zheng, B. Zhou, F. Long, Synthesis, structure, and photoelectric properties of novel 0-dimensional organic-inorganic hybrid perovskite (2-5-py)$_2$$MnBr_4$, J. Phys. Chem. C 125 (2021) 22898–22906.

[21] Y. Qin, P. She, X. Huang, W. Huang, Q. Zhao, Luminescent manganese(II) complexes: Synthesis, properties and optoelectronic applications, Coord. Chem. Rev. 416 (2020), 213331.

[22] P. Tao, S.-J. Liu, W.-Y. Wong, Phosphorescent manganese(II) complexes and their emerging applications, Adv. Opt. Mater. 8 (2020) 2000985.

[23] D.M.L. Goodgame, F.A. Cotton, Phosphine oxide complexes. Part V. Tetrahedral complexes of manganese(II) containing triphenylphosphine oxide, and triphenylarsine oxide as ligands, J. Chem. Soc. (1961) 3735–3741.

[24] B.P. Chandra, B.R. Kaza, Mechanoluminescence, electroluminescence and high-pressure photoluminescence of Mn$(Ph_3PO)_2$Br 2, J. Lumin. 27 (1) (1982) 101–107.

[25] F.A. Cotton, L.M. Daniels, P. Huang, Correlation of structure and triboluminescence for tetrahedral manganese(II) compounds, Inorg. Chem. 40 (14) (2001) 3576–3578.

[26] Y.-Y. Tang, Z.-X. Wang, P.-F. Li, Y.-M. You, A. Stroppa, R.-G. Xiong, Brilliant triboluminescence in a potential organic–inorganic hybrid ferroelectric: $(Ph_3PO)_2MnBr_2$, Inorg. Chem. Front. 4 (1) (2017) 154–159.

[27] X. Huang, Y. Qin, P. She, H. Meng, S. Liu, Q. Zhao, Functionalized triphenylphosphine oxide-based manganese(II) complexes for luminescent printing, Dalton Trans. 50 (2021) 8831–8836.

[28] A.V. Artem'ev, M.P. Davydova, A.S. Berezin, V.K. Brel, V.P. Morgalyuk, I. Yu Bagryanskaya, D.G. Samsonenko, Luminescence of the Mn^{2+} ion in non-O_h and T_d coordination environments: the missing case of square pyramid, Dalton Trans. 48 (2019) 16448–16456.

[29] M. Bortoluzzi, J. Castro, E. Trave, D. Dallan, S. Favaretto, Orange-emitting manganese(II) complexes with chelating phosphine oxides, Inorg. Chem. Commun. 90 (2018) 105–107.

[30] A.S. Berezin, M.P. Davydova, I.Y. Bagryanskaya, O.I. Artyushin, V.K. Brel, A. V. Artem'ev, A red-emitting Mn(II)-based coordination polymer build on 1,2,4,5-tetrakis(diphenylphosphinyl)benzene, Inorg. Chem. Commun. 107 (2019), 107473.

[31] J. Chen, Q. Zhang, F.-K. Zheng, Z.-F. Liu, S.-H. Wang, A.-Q. Wu, G.-C. Guo, Intense photo- and tribo-luminescence of three tetrahedral manganese(II) dihalides with chelating bidentate phosphine oxide ligand, Dalton Trans. 44 (2015) 3289–3294.

[32] Y. Wu, X. Zhang, L.-J. Xu, M. Yang, Z.-N. Chen, Luminescent vapochromism due to a change of the ligand field in a one-dimensional manganese(II) coordination polymer, Inorg. Chem. 57 (15) (2018) 9175–9181.

[33] A.S. Berezin, D.G. Samsonenko, V.K. Brel, A.V. Artem'ev, "Two-in-one" organic–inorganic hybrid Mn^{II} complexes exhibiting dual-emissive phosphorescence, Dalton Trans. 47 (21) (2018) 7306–7315.

[34] Y. Wu, X. Zhang, Y.-Q. Zhang, M. Yang, Z.-N. Chen, Achievement of ligand-field induced thermochromic luminescence via two-step single-crystal to single-crystal transformations, Chem. Commun. 54 (99) (2018) 13961–13964.

[35] M.P. Davydova, I.A. Bauer, V.K. Brel, M.I. Rakhmanova, I.Y. Bagryanskaya, A. V. Artem'ev, Manganese(II) thiocyanate complexes with bis(phosphine oxide) ligands: synthesis and excitation wavelength-dependent multicolor luminescence, Eur. J. Inorg. Chem. (2020) 695–703.

[36] A.V. Artem'ev, M.P. Davydova, A.S. Berezin, T.S. Sukhikh, D.G. Samsonenko, Photo- and triboluminescent robust 1D polymers made of Mn(II) halides and *meta*-carborane based bis(phosphine oxide), Inorg. Chem. Front. 8 (2021) 2261–2270.

[37] A.V. Artem'ev, M.P. Davydova, M.I. Rakhmanova, I.Y. Bagryanskaya, D. P. Pishchur, A family of Mn(II) complexes exhibiting strong photo- and triboluminescence as well as polymorphic luminescence, Inorg. Chem. Front. 8 (2021) 3767–3774.

[38] Y.Y. Qin, P. Tao, L. Gao, P.F. She, S.J. Liu, X.L. Li, F.Y. Li, H. Wang, Q. Zhao, Y. Q. Miao, W. Huang, Designing highly efficient phosphorescent neutral tetrahedral manganese(II) complexes for organic light-emitting diodes, Adv. Opt. Mater. 7 (2019) 1801160.

[39] H. Meng, W. Zhu, F. Li, X. Huang, Y. Qin, S. Liu, Y. Yang, W. Huang, Q. Zhao, Highly emissive and stable five-coordinated manganese(II) complex for X-ray imaging, Laser Photonics Rev. 15 (11) (2021) 2100309.

[40] M. Bortoluzzi, J. Castro, A. Di Vera, A. Palù, V. Ferraro, Manganese(II) bromo- and iodo-complexes with phosphoramidate and phosphonate ligands: synthesis, characterization and photoluminescence, New J. Chem. 45 (2021) 12871–12878.

[41] M. Bortoluzzi, J. Castro, F. Enrichi, A. Vomiero, M. Busato, W. Huang, Green-emitting manganese(II) complexes with phosphoramide and phenylphosphonic diamide ligands, Inorg. Chem. Commun. 92 (2018) 145–150.

[42] M. Bortoluzzi, J. Castro, Dibromomanganese(II) complexes with hexamethylphosphoramide and phenylphosphonic bis(amide) ligands, J. Coord. Chem. 72 (2019) 309–327.

[43] M. Bortoluzzi, J. Castro, A. Gobbo, V. Ferraro, L. Pietrobon, S. Antoniutti, Tetrahedral photoluminescent manganese(II) halide complexes with 1,3-dimethyl-2-phenyl-1,3-diazaphospholidine-2-oxide as a ligand, New J. Chem. 44 (2020) 571–579.

[44] M. Bortoluzzi, J. Castro, A. Gobbo, V. Ferraro, L. Pietrobon, Light harvesting indolyl-substituted phosphoramide ligand for the enhancement of Mn(II) luminescence, Dalton Trans. 49 (2020) 7525–7534.

[45] M. Bortoluzzi, V. Ferraro, J. Castro, Synthesis and photoluminescence of manganese(II) naphtylphosphonic diamide complexes, Dalton Trans. 50 (2021) 3132–3136.

[46] Z. Zhao, G. Yu, Q. Chang, X. Liu, Y. Liu, L. Wang, Z. Liu, Z. Bian, W. Liu, C. Huang, Carbazolylphosphines and carbazolylphosphine oxides: facilely synthesized host materials with tunable mobilities and high triplet energy levels for blue phosphorescent OLEDs, J. Mater. Chem. C 5 (2017) 7344–7351.

[47] A. Wada, T. Yasuda, Q. Zhang, Y.S. Yang, I. Takasu, S. Enomoto, C. Adachi, A host material consisting of a phosphinic amide directly linked donor–acceptor structure

for efficient blue phosphorescent organic light-emitting diodes, J. Mater. Chem. C 1 (13) (2013) 2404.
[48] Y. Tao, J. Xiao, C. Zheng, Z. Zhang, M. Yan, R. Chen, X. Zhou, H. Li, Z. An, Z. Wang, H. Xu, W. Huang, Dynamically adaptive characteristics of resonance variation for selectively enhancing electrical performance of organic semiconductors, Angew. Chem. Int. Ed. 52 (40) (2013) 10491–10495.
[49] W.L.F. Armarego, D.D. Perrin, Purification of Laboratory Chemicals, 4th ed., Butterworth-Heinemann, Oxford, 1996.
[50] M. Bortoluzzi, A. Gobbo, A. Palù, F. Enrichi, A. Vomiero, Luminescent lanthanide complexes with phosphoramide and arylphosphonic diamide ligands, Chem. Pap. 74 (11) (2020) 3693–3704.
[51] D.J. Pietrzyk, C.W. Frank, Analytical Chemistry, 2nd ed., Academic Press, New York, 2012.
[52] G.A. Bain, J.F. Berry, Diamagnetic corrections and Pascal's constants, J. Chem. Educ. 85 (4) (2008) 532, https://doi.org/10.1021/ed085p532.
[53] APEX3, SMART, SAINT, Bruker AXS Inc., Madison, Wisconsin, USA, 2015.
[54] P. McArdle, Oscail, a program package for small-molecule single-crystal crystallography with crystal morphology prediction and molecular modelling, J. Appl. Crystallogr. 50 (1) (2017) 320–326.
[55] G.M. Sheldrick, SHELXT – Integrated space-group and crystal-structure determination, Acta Crystallogr, Sect. A: Found. Crystallogr. 71 (1) (2015) 3–8.
[56] G.M. Sheldrick, Crystal structure refinement with SHELXL, Acta Crystallogr, Sect. C: Struct. Chem. 71 (2015) 3–8.
[57] A.L. Spek, checkCIF validation ALERTS: what they mean and how to respond, Acta Crystallogr. E 76 (2020) 1–11.
[58] H.S. Yu, X. He, S.L. Li, D.G. Truhlar, MN15: a Kohn-Sham global-hydrid exchange-correlation density functional with broad accuracy for multi-reference and single-reference systems and noncovalent interactions, Chem. Sci. 7 (2016) 5032–5051.
[59] F. Weigend, R. Ahlrichs, Balanced basis sets of split valence, triple zeta valence and quadruple zeta valence quality for H to Rn: Design and assessment of accuracy, Phys. Chem. Chem. Phys. 7 (18) (2005) 3297.
[60] C.J. Cramer, Essentials of Computational Chemistry, 2nd ed., Wiley, Chichester, 2004.
[61] Gaussian 16, Revision C.01, M.J. Frisch, G.W. Trucks, H.B. Schlegel, G.E. Scuseria, M.A. Robb, J.R. Cheeseman, G. Scalmani, V. Barone, G.A. Petersson, H. Nakatsuji, X. Li, M. Caricato, A.V. Marenich, J. Bloino, B.G. Janesko, R. Gomperts, B. Mennucci, H.P. Hratchian, J.V. Ortiz, A.F. Izmaylov, J.L. Sonnenberg, D. Williams-Young, F. Ding, F. Lipparini, F. Egidi, J. Goings, B. Peng, A. Petrone, T. Henderson, D. Ranasinghe, V.G. Zakrzewski, J. Gao, N. Rega, G. Zheng, W. Liang, M. Hada, M. Ehara, K. Toyota, R. Fukuda, J. Hasegawa, M. Ishida, T. Nakajima, Y. Honda, O. Kitao, H. Nakai, T. Vreven, K. Throssell, J.A. Montgomery, Jr., J.E. Peralta, F. Ogliaro, M.J. Bearpark, J.J. Heyd, E.N. Brothers, K.N. Kudin, V.N. Staroverov, T.A. Keith, R. Kobayashi, J. Normand, K. Raghavachari, A.P. Rendell, J.C. Burant, S.S. Iyengar, J. Tomasi, M. Cossi, J.M. Millam, M. Klene, C. Adamo, R. Cammi, J.W. Ochterski, R.L. Martin, K. Morokuma, O. Farkas, J.B. Foresman, D.J. Fox, Gaussian, Inc., Wallingford CT, 2019.
[62] C.F. Macrae, I. Sovago, S.J. Cottrell, P.T.A. Galek, P. McCabe, E. Pidcock, M. Platings, G.P. Shields, J.S. Stevens, M. Towler, P.A. Wood, Mercury 4.0: from visualization to analysis, design and prediction, J. Appl. Cryst. 53 (2020) 226–235.
[63] POV-Ray v3.7 for Windows, Persistence of Vision Pty. Ltd., 2016, Persistence of Vision Raytracer (Version 3.7), http://www.povray.org/.
[64] L. Yang, D.R. Powell, R.P. Houser, Structural variation in copper(I) complexes with pyridylmethylamide ligands: structural analysis with a new four-coordinate geometry index, τ_4, Dalton Trans. 955–964 (2007).
[65] A. Okuniewski, D. Rosiak, J. Chojnacki, B. Becker, Coordination polymers and molecular structures among complexes of mercury(II) halides with selected 1-benzoylthioureas, Polyhedron 90 (2015) 47–57.
[66] C.R. Groom, I.J. Bruno, M.P. Lightfoot, S.C. Ward, The Cambridge structural database, Acta Cryst. B 72 (2) (2016) 171–179.
[67] X. Liu, R. Dronskowski, R. Glaum, A.L. Tchougréeff, Experimental and Quantum-Chemical Investigations of the UV/Vis Absorption Spectrum of Manganese Carbodiimide, MnNCN, Z. Anorg. Allg. Chem. 636 (2) (2010) 343–348.
[68] K. Li, Y. Chen, J. Wang, C. Yang, Diverse emission properties of transition metal complexes beyond exclusive single phosphorescence and their wide applications, Coord. Chem. Rev. 433 (2021), 213755.
[69] S.K. Behera, S.Y. Park, J. Gierschner, Dual emission: classes, mechanisms, and conditions, Angew. Chem. Int. Ed. 60 (42) (2021) 22624–22638.
[70] Z. He, W. Zhao, J.W.Y. Lam, Q. Peng, H. Ma, G. Liang, Z. Shuai, B.Z. Tang, White light emission from a single organic molecule with dual phosphorescence at room temperature, Nat. Commun. 8 (2017) 416.
[71] T. Wang, X. Su, X. Zhang, X. Nie, L. Huang, X. Zhang, X. Sun, Y. Luo, G. Zhang, Aggregation-induced dual-phosphorescence from organic molecules for nondoped light-emitting diodes, Adv. Mater. 31 (2019) 1904273.
[72] H. Wang, J. Wang, T. Zhang, Z. Xie, X. Zhang, H. Sun, Y. Xiao, T. Yu, W. Huang, Breaching Kasha's rule for dual emission: mechanisms, materials and applications, J. Mater. Chem. C 9 (32) (2021) 10154–10172.
[73] M. Wrighton, D. Ginley, Excited state decay of tetrahalomanganese(II) complexes, Chem. Phys. 4 (2) (1974) 295–299.
[74] H. Yersin, A.F. Rausch, R. Czerwieniec, T. Hofbeck, T. Fischer, The triplet state of organo-transition metal compounds. Triplet harvesting and singlet harvesting for efficient OLEDs, Coord. Chem. Rev. 255 (21-22) (2011) 2622–2652.